The evolution of deep convective systems and their associated cirrus outflows

George Horner[1] and Edward Gryspeerdt[1,2]

[1]Space and Atmospheric Physics Group, Imperial College London, London, UK
[2]Grantham Institute - Climate Change and the Environment, Imperial College London, London, UK

Correspondence: George Horner (g.horner20@imperial.ac.uk)

Abstract.

Tropical deep convective clouds, particularly their large cirrus outflows, play an important role in modulating the energy balance of the Earth's atmosphere. Whilst the cores of these deep convective clouds have a significant shortwave (SW) cooling effect, they dissipate quickly. Conversely, the thin cirrus that flow from these cores can persist for days after the core has dissipated, reaching hundreds of kilometers in extent. These thin cirrus have a potential for large warming in the tropics. Understanding the evolution of air parcels from deep convection, clouds along these trajectories, and how they change in response to anthropogenic emissions is therefore important to understand past and future climate change.

This work uses a novel approach to investigate the evolution of tropical convective clouds by introducing the concept of 'Time Since Convection' (TSC). This is used to build a composite picture of the lifecycle of air parcels from deep convection. Cloud properties are a strong function of TSC, showing decreases in the optical thickness, cloud top height, and cloud fraction over time, driving the latitudinal structure of cloudiness. After an initial dissipation of the convective core, changes in thin cirrus cloud amount were seen beyond 200 hours from convection. Changes in cloud are shown to be a strong function of TSC, and not simply reflective of latitudinal changes as air moves from the tropics to the extra tropics.

Finally, in the initial stages of convection there was a large net negative cloud radiative effect (CRE). However, once the convective core had dissipated, the sign of the CRE flipped, and there was a sustained net warming CRE beyond 120 hours from the convective event. Changes are present in the cloud properties long after the main convective activities have dissipated, signalling the need to continue further analysis at longer time scales than previously studied.

1 Introduction

Deep convective clouds (DCC) occur primarily in the tropical and subtropical regions. They are characterized by one or more convective cores (cumulus towers), with strong updrafts that merge the cores at higher altitudes and large anvils flowing out from the region of convection (Fan et al., 2013). The radiative forcing from deep convective cores in the tropics can vary greatly depending on the optical thickness and ice water path of the cloud (Berry and Mace, 2014; Hartmann and Berry, 2017). However, the overall total cloud radiative effect (CRE) in the tropics is small (Wielicki et al., 1996). This is due to the cancellation of the large (longwave) LW warming that occurs in cloudy regions in the tropics, and the significant SW CRE that

comes from the high albedo of these same regions. This leads to the CRE in cloudy regions of the tropics being very similar to the CRE in nearby non-convective regions (Hartmann and Berry, 2017; Harrison et al., 1990; Ramanathan et al., 1989).

Whether this cancellation is due to feedbacks or is simply a coincidence is unclear (Kiehl, 1994; Hartmann et al., 2001b). If a coincidence, then the behaviour of these deep convective regimes may change in a warming world, or under different aerosol concentrations. This cancellation is the sum of large SW and LW components. Therefore any small change in either of these components could potentially have a large effect on the overall CRE. Understanding the lifecycle and drivers of deep convection is thus important to understand the sensitivity of these regimes.

Whilst the convective cores alone have a negative CRE, their lifetimes are relatively short in comparison to the outflowing anvil cirrus. Hartmann et al. (2001b) found that the TOA radiative forcing of DCC ranged between +20 to -119 Wm^{-2}, with the optical depth of tropical DCC ranging from 1 to 60 in the upper troposphere. On the other hand, the detrained thin cirrus from the anvil of the top of convective core can persist up to 5 days (Luo and Rossow, 2004), cover large spatial extents and have a significant warming contribution to the CRE (Protopapadaki et al., 2017; Wall et al., 2018).

The sign of the radiative forcing from cirrus in the tropics is highly dependent on the optical thickness of the cloud (τ_c). Choi and Ho (2006) found that thin cirrus between 10-12km with an optical depth $\tau_c < 10$ have a warming effect, whilst cirrus with $\tau_c > 10$ have a cooling effect. Koren et al. (2010) showed that the cloud top height also plays a vital role in the sign of the forcing from cirrus. They showed that if the cirrus cloud top height is increased and optical depth decreased, there is potential for much greater warming.

The lifecycle of deep convective and their associated anvil and thin cirrus outflows has been investigated in numerous prior works, both in observations and models. Using observational data, Luo and Rossow (2004) found that 50% of of tropical cirrus clouds originated from convection. They found that the detrained cirrus had, on average, longer lifetimes than the in-situ cirrus, at around 30 hours compared to 19 hours for in-situ. This suggests some mechanism for sustaining water vapour at the detrained cirrus height that allows for the longer lifetimes. Using ground based data and satellites, Mace et al. (2006) found that 47% of cirrus observed over Manus island in the western Pacific originated from deep convection occurring within the past 12 hours. Many other modelling and observational studies also show that at least 50% of tropical cirrus originate from convection (Massie et al., 2002; Gehlot and Quaas, 2012; Riihimaki et al., 2012). Salathé and Hartmann (1997) showed that upper tropospheric humidity is sustained for up to 5 days from convection. This is consistent with the cirrus decay found by Luo and Rossow (2004).

Garrett et al. (2005) looked at the detailed evolution of a single thunderstorm anvil cirrus cloud in Florida. They found that the advected outflow was separated into two cloud layers; a cirrus anvil at -45°C lying below a thin tropopause cirrus (TCC) at -70°C. The TCC lifetime was sustained longer than that of the anvil cirrus, potentially due to anvil cirrus shielding the TCC from terrestrial radiation, as proposed by Hartmann et al. (2001a). Schwartz and Mace (2010) used CloudSat and CALIPSO data to examine this mechanism. For a complete overview of the different cirrus types and their origin, Krämer et al. (2016) synthesised multiple field campaigns, simulations and model results looking at cirrus microphysics, splitting up in situ, detrained, liquid origin, and TTL cirrus.

Studies investigating the model evolution of cirrus found broadly similar results to those found in observations. Gehlot and Quaas (2012) saw a rapid decay (6-12hrs) of deep convection from the peak, and an associated growth of cirrus in the ECHAM5 model. After one day they found a decay of the cirrostratus, likely associated with a loss of cloud water due to larger particles that have a large sedimentation mass flux. Jensen et al. (2018) investigated the detrainment of ice crystals from the tops of deep convection in a cloud resolving model (CRM). They found that most large ice crystals (>200μm in diameter) fall out of the anvils within 2 hours of formation. The cirrus decay was much slower, occurring over 120 hours, from a maximum cirrus cloud fraction of 0.4 to 0.15 after 120 hours. They also looked at changes under increased SSTs, finding anvil cirrus clouds having increased cloud fractions, and higher cloud tops, leading to a positive cloud feedback.

When considering the CRE of the evolution of the convective system, it is the balance between the LW and SW over the entire lifetime of the cirrus in the tropics that, if perturbed, could lead to large changes in the overall net CRE. Most tropical radiative studies are confined to models. Looking at the CRE along Lagrangian trajectories in simulation, Gasparini et al. (2021) found that large SW and LW values dominate close to convection as expected. The net CRE oscillates close to zero and is a function of the solar insolation. In their simulations most convection occurs in the early morning, there is a peak in net negative CRE at peak solar insolation when SW cooling dominates. There is a slight warming at 15 hours, when the anvil has thinned sufficiently and the solar insolation decreased enough for the LW CRE to dominate.

The factors that control the radiative evolution of the decaying cirrus have also been investigated in model studies. Gasparini et al. (2019) found that at high (>100gm^{-2}) IWP values, or above the 80th percentile, the net CRE is negative. Beyond this, at low IWP and correspondingly low cloud fractions above 12km the net CRE switches signs to a small positive value. This switch occurs when the τ_c is around 4, roughly where precipitation stops occurring. This is a lower value for the τ_c than found in observations by Choi and Ho (2006). As the CF and IWP decrease, the CRE tends to zero. The switch from warming to cooling happens at around 6 hours from convection in Gasparini et al. (2019). They generally found that small scale microphysical and dynamical processes are responsible for determining the lifecycle of the detrained anvil cloud. Current GCMs have too coarse horizontal and vertical resolutions to accurately reflect the dynamical processes controlling anvil cirrus evolution (Wall and Hartmann, 2018).

Most previous work focused on individual mesoscale studies and capped the analysis at shorter time scales in the region of 120 hours. In contrast, this paper presents a method to run a Lagrangian trajectory analysis across the entire tropics at unbounded trajectory lengths at a low computational cost, leading to changes being found in the cloud properties at time scales far beyond 120 hours after the initial convection has dissipated. Used in conjunction with lidar and radar data, the vertical evolution of the cloud properties are characterised as a function of time since convection. The approach in this work builds a composite picture of the lifecycle tropical convective into thin cirrus. This paper also investigates how TSC is a function of latitude, and shows that the changes in the cloud properties along trajectories are a strong function of TSC and are not simply reflective of latitudinal changes as air moves from the tropics to the extratropics. This paper also considers the radiative evolution for just the high clouds along the trajectories.

2 Method

2.1 Data

Observational data from the 3-hourly International Satellite Cloud Climatology Project (ISCCP) H dataset at 1x1° is used to define locations of deep convection (Rossow et al., 2017). ECMWF ERA5 reanalysis wind fields are used in the trajectory analysis (Hersbach et al., 2018) and to characterise cloud properties. To examine the evolution of the radiative properties, the CERES SYN1deg L3 LW and SW TOA fluxes are used (NASA/LARC/SD/ASDC, 2017). The CERES SYN1deg product combines MODIS and geostationary satellite data to provide global coverage at a 1x1° resolution and 1 hourly temporal resolution. The vertical evolution of the cloud is investigated by utilising the DARDAR dataset, which is an ice cloud retrieval product that combines measurements from the CloudSat radar and CALIPSO lidar (Delanoë and Hogan, 2008; Sourdeval et al., 2018). The period of study in this paper is 2008-2010 inclusive.

2.2 Convective core identification

In order to track the time since a parcel of air last experienced convection, convective cores were defined and identified in the satellite data. This work uses the global weather states in Tselioudis et al. (2021), which uses the ISCCP-H 1 by 1° daytime and nighttime 3 hourly dataset (Rossow et al., 2017). The ISCCP-H differs from prior ISCCP products in numerous ways, most importantly improving the spatial resolution to 1° from 2.5°. A full list of the differences in the data products is given in (Rossow et al., 2017). The ISCCP-H dataset is separated into seven distinct cloud regimes by calculating the nearest neighbours of each gridbox and clustering them into the separate regimes depending on their cloud fraction, albedo, and cloud top pressure. These cloud regimes, and their associated centroid values, are shown in Table 1. The albedo is calculated from the optical thickness using Eq. 1.

$$\alpha = \frac{\tau_c^{0.895}}{\tau_c^{0.895} + 6.82} \tag{1}$$

as defined in the ISCCP simulator (Klein and Jakob, 1999). For a full description of the ISCCP-H weather states, see Tselioudis et al. (2021).

This study is focused on the tropical region of 30S-30N and only considers the deep convection defined within the tropics, whereas the weather states in Table 1 are defined globally. Note that the value of 10.5 for the optical depth centroid for the deep convection is typically lower than the optical depth of deep convective cores in high resolution satellite data. The ISCCP data used here is at 1x1°, and therefore the bins will have a lower average optical depth across the whole gridbox.

Additional conditions are applied to isolate the convective cores, requiring a $\tau_c > 8.5$ (albedo > 0.5) and a cloud top temperature (CTT) < 220K. Only the very brightest, thickest cores of the convective clouds are categorised as DCC. If these conditions aren't imposed then thick anvil cirrus are included as part of the convective cores, and the ability to investigate their temporal development is reduced.

Regime	CTP / hPa	τ_c	CF / %
Deep convective cores	**242.6**	**10.5**	**99.5**
Mid latitude storm	433.6	10.4	99.2
Thin high cirrus	316.3	1.2	79.9
Polar	395.6	2.2	84.5
Middle top clouds	606.9	9.5	97.2
Fair weather	645.1	3.2	40.0
Shallow cumulus	840.1	4.0	79.6
Stratocumulus	725.5	6.3	90.7

Table 1. ISCCP-H cloud regime centroid values for the CTP, τ_c, and CF from Tselioudis et al. (2021). The deep convective cloud regime, DCC, is highlighted in bold.

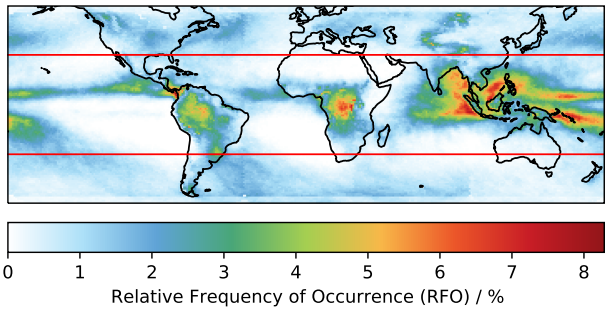

Figure 1. Relative frequency of occurrence (RFO) of the convective core regime from between 2007-2010. Red bands show the boundaries of the tropics (30S-30N).

The mean relative frequency of occurrence (RFO) for the convective cores for the years 2007-10 is shown in Fig. 1. Most of the convection occurs in the Maritime Continent, over Central Africa, South America, and along the ITCZ. This work is only concerned with tropical convection, defined in the region between the red boundaries (30S-30N).

2.3 Time Since Convection

The ECMWF ERA5 reanalysis wind speeds at 0.25° are used in this study (Hersbach et al., 2018). A pressure averaged wind field between 200hPa and 300hPa is used to advect the convective cores forward, in order to best reflect the range of heights that the convective cores and subsequent detrained cirrus exist. This is the same logic as applied in Luo and Rossow (2004), where vertical movement of air is not considered, however they use a pressure averaged wind field between 200hPa and 500hPa. The decision to use a higher altitude average wind field is addressed in section 2.5.

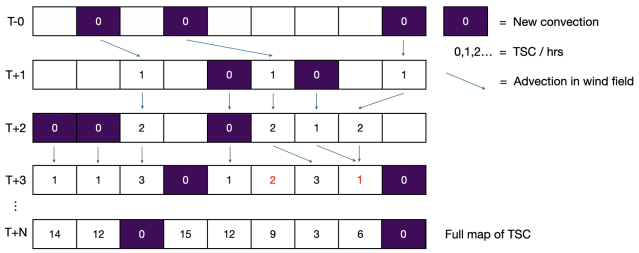

Figure 2. Schematic diagram of the advection process in one dimension, assuming all locations start with no TSC value. Red values indicate where either a divergence or convergence of pixels occurs. The purple boxes show new convection occuring, and the arrows highlight the advection of convective air into new gridboxes between timesteps. The values of the TSC are shown in each box.

The advection process is as follows. All the pixels in the tropics are advected forward one hour in time according to the wind field. The TSC now has values of T+1 hours since convection. In locations where DCC are present, the TSC is reset to zero. This advection process repeats, each time resetting locations of DCC to zero TSC. Fig. 2 show a schematic diagram of the process in one dimension.

The TSC algorithm runs at 0.1x0.1° resolution. Running the TSC code at 0.1x0.1° is necessary to ensure that between one hour timesteps there is a high enough resolution so that parcels are advected out of the pixels they currently occupy. If the algorithm was run at 1x1°, large discretisation errors would be introduced, as air would very rarely travel out of the pixel that it occupies within a single hour-long timestep. For this reason, the resolution of the DCC dataset is increased to 0.1x0.1° using a nearest-neighbour interpolation to be compatible with the TSC algorithm. The resolution of the outputted TSC files is averaged to 1x1° to be compatible with the MODIS and CERES gridded products..

The TSC array is interpolated into missing regions after each advection timestep (Fig. 2). When each 0.1x0.1° pixel in the TSC array is advected forward, some of the trajectories converge to occupy the same pixel, necessarily leaving some pixels without a TSC value. When this occurs, the missing values are interpolated as an average of TSC values around this empty pixel. Between each timestep, divergence leaves approximately 5% of the pixels empty. When two trajectories enter the same pixel, they will proceed to follow the same trajectory ad infinitum due to the deterministic nature of the trajectories. Therefore the trajectory with the smaller TSC value is the one that determines the TSC value at that pixel from that point on. This increases confidence that any high TSC value really represents air at such long timescales since convection.

The TSC map is defined between 32S-32N to ensure that air is allowed to briefly leave the region of analysis and reenter. If the wind field brings air from outside 32S-32N into this region, this new air will not be assigned a TSC value until it meets new convection or advection introduces a TSC value. This increases confidence in the high TSC regions. If TSC is defined well beyond the tropics, the extratropics act like a reservoir of very high TSC values that are occasionally advected back into the tropics. This inflates the TSC values, because no convection is defined outside of 30S-30N.

As TSC is initially undefined, there is an associated spin up time until every point is a true reflection of the hours since the air at that location last experienced convection. This spin up time is shown in Fig. 3 and is approximately 20 days. Therefore in all further analysis, the first month of data are excluded.

2.4 Evaluation of TSC

After the spin up, there is minimal variability in the TSC across two years of data, with the mean TSC oscillating around 180 hours (Fig. 3). The 10th percentile is very consistent, due to the regularity of new convection occurring in the dataset. The 90th percentile is more erratic, oscillating between 350 hours and occasionally over 500 hours, due to the sporadic nature of the occurrence of very high TSC regions and the long tail on the distribution of TSC.

It is interesting to note that the 90th percentile TSC values are considerably higher than the temporal length of the trajectories in prior works (Gehlot and Quaas, 2012; Luo and Rossow, 2004). Both of these studies limited their analysis to 120 hours (5 days), which included only 30% of tropical locations (Fig.3b). This is a benefit of the TSC approach, which allows the trajectories to be computationally efficiently advected without an upper bound to their length, so does not bias the results towards shorter trajectories.

2.5 Comparison with HYSPLIT trajectories

A comparison can be made to individual trajectories initiated from locations of convection. The HYSPLIT Lagrangian forward trajectory model is used in this paper (Rolph et al., 2017). The HYSPLIT model uses reanalysis data from NCEP/NCAR to advect individual air parcels in a 3D wind field, which includes vertical transport of the air parcel. In this work, HYSPLIT trajectories are initiated from the centre of each 1x1° box that contains a TSC-0 value, at an altitude of 10km. This altitude is between approximately 300hPa in the tropics. These trajectories are followed for 315 hours, with the TSC time at the location of each trajectory compared the time since the HYSPLIT trajectories were initiated. This is done for three complete days across 2008 (Jan 1st, Jun 1st, and Sept 1st). Fig. 4 shows the median value of the TSC for the gridbox occupied by the trajectories. The dotted red line indicates all the trajectories initiated from the convective cores (1033 in total), ignoring any new convection along that trajectory. The solid blue line only includes trajectories up to the point at which they next experience convection, which better represents the TSC methodology.

The TSC value and HYSPLIT trajectory time broadly match for lower TSC values (Fig. 4). However, particularly for the trajectories that stop when they experience new convection, the TSC values are higher than the time since the trajectories are initiated. The main reason for this difference is there is no vertical transport in the TSC advection algorithm. Rather, the average wind speeds between 200hPa-300hPa are used to advect the air parcels. The trajectories in the NCEP/NCAR HYSPLIT model are initiated at an average pressure of 200hPa. This height is an approximation of the DCC detrainment altitude, which leads to some uncertainty in the relevant wind level for advection. During the early stages of the HYSPLIT trajectory, the HYSPLIT wind speed will be greater than that used for the TSC trajectory. This is because the HYSPLIT trajectory is at 200hPa and the TSC trajectory wind speed is averaged between the 200hPa and 300hPa wind speeds.

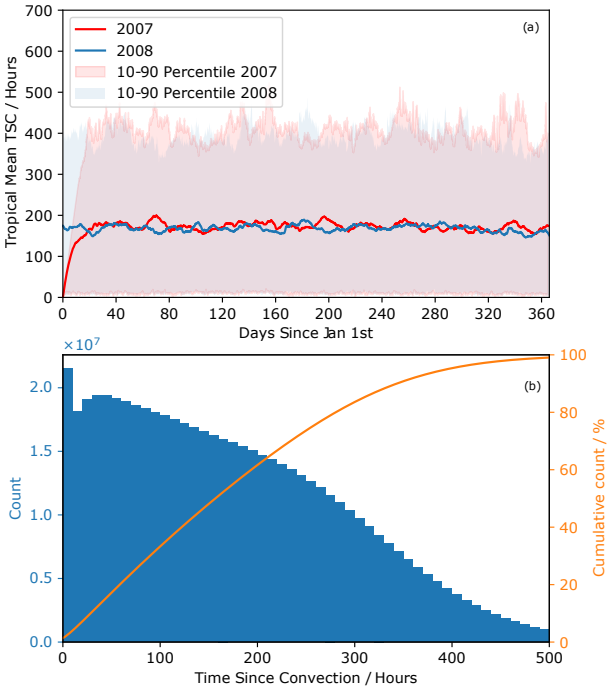

Figure 3. a) Tropical mean Time Since Convection (TSC) for 2007 and 2008, with 10th-90th percentiles highlighted. The top right histogram shows the normalised distribution of TSC values over the 2 year period, excluding the spin up time. There is little variation in the mean TSC between the years after the initial spin up period in 2007. b) Histogram of TSC values between 2007-2010 between 0 and 500 hours. Right axis shows the cumulative distribution in percentage of all TSC values. >99% of TSC values are less than 500 hours.

185 This explains why the TSC is greater than the age of the trajectories, as the faster HYSPLIT winds will move further from convection than modelled by the TSC dataset. As the trajectories subside (it is worth noting that there is uncertainty in the appropriate subsidence rate), the horizontal wind speeds decrease, and start to become closer to the wind speeds in the TSC dataset, therefore the difference between the age of the trajectories and the TSC becomes constant. As the trajectories begin to subside even more, the TSC values become closer to the age of the trajectories, until at around 150 hours where the TSC value 190 becomes lower than the age of the trajectories. This close comparison between the TSC and HYSPLIT trajectory times justifies the use of the 200-300hPa pressure levels, rather than the broader range of pressure levels used by Luo and Rossow (2004).

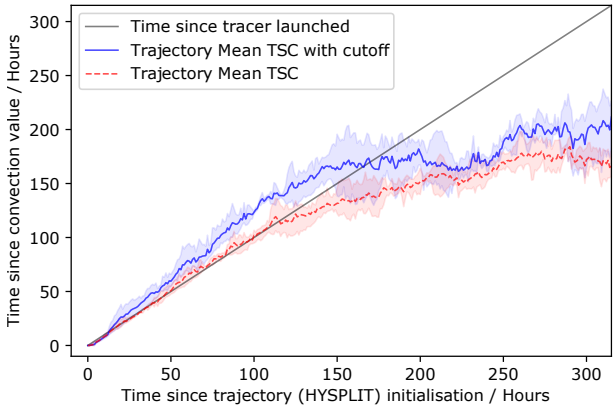

Figure 4. Median TSC values (y-axis) along HYSPLIT trajectories (x-axis), for all trajectories and for trajectories that are stopped once they reach new convection. Error range between maximum to minimum trajectory values. Straight line indicates an exact relationship between trajectory age and TSC value.

2.6 Cloud Properties

The ISCCP-H dataset is used to investigate how the CTP and τ_c change as a function of TSC, making use of the joint histograms of CTP-$\tau_c$in the ISCCP product. These show cloud fraction for a range of CTP and τ_c bins, produced at the pixel-level and limited to show the evolution of the tropical gridbox mean values for the region between 30S-30N. The joint histograms are used to isolate the highest clouds, retaining only the top 3 CTP bins of the histogram (>375hPa). This is done by multiplying the centroid value of the top 3 CTP bins by the cloud fraction of each bin from the joint histograms. This allows for a comparison for the evolution of the τ_c and CTP for all clouds, and just the highest clouds in the tropics.

Failed retrievals in the ISCCP-H dataset, are assigned to the lowest τ_c and CTP bin in the joint histogram. The bin containing these missing values significantly affect the high cloud τ_c and CTP, so is removed when generating the τ_c and CTP histograms in Fig. 7.

The vertical profile of the cirrus is investigated using the DARDAR dataset, a combination of the CloudSat radar and CALIPSO lidar (Delanoë and Hogan, 2008). The overpass locations of DARDAR are matched within the hour to the TSC at that location, at 1x1° resolution. A 1x1° can contain many DARDAR retrievals, each of these DARDAR retrievals is assigned the same TSC value - that of the 1x1° gridbox. These DARDAR retrievals then all contribute equally to the analysis in the relevant TSC bin The DARDAR cloud mask is used to filter out aerosol, ground, and unknown retrievals. The DARDAR-Nice product (Sourdeval et al., 2018; **?**) is used to provide the vertical profile of ice crystal number concentration (N_i) for crystals larger than 5um (N_i^5) and larger than 100um (N_i^{100}).

The radiative evolution of convection, from thick convective core to thin anvil cirrus, is investigated by analysing the CERES SYN1deg L3 LW and SW TOA fluxes (NASA/LARC/SD/ASDC, 2017). The CRE is calculated as the all sky minus clear sky radiative fluxes from the CERES data. In order to only look at the radiative evolution of the highest clouds, regions where the

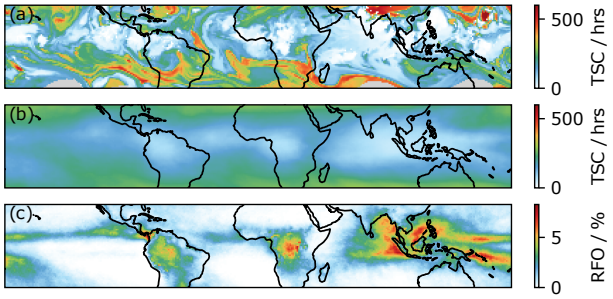

Figure 5. a) Snapshot of the TSC 30S-30N at 00:30UTC 26th July 2008. b) Mean TSC for between 2008-2010. c) RFO of deep convection between 2008-2010 (as in Fig. 1).

cloud fraction of the low clouds (as defined by the ISCCP joint histograms) is less than 1% are classified as "high cloud only "gridboxes. For the cloudiest regions in the tropics (which are also the regions of the lowest TSC), there is often no hourly outgoing clear sky LW data. For these gridboxes, the 3 monthly seasonal average outgoing clear sky LW for these gridboxes is used, in order to calculate a value for the CRE.

The ISCCP histograms used to isolate the high clouds are only available during daylight, such that the high cloud only CRE is only available during daylight. However, the SW is known to be zero during the night, so the nighttime values for the SW CRE are included in the analysis as zero. The daytime LW values are assumed representative of the nighttime values.

3 Results

3.1 Regional distribution of Time Since Convection.

Fig. 5 shows the map of time since convection for the tropical region 30S-30N at 00:30 UTC on Jan 1st 2008. As might be expected, the TSC map broadly follows the geographical distribution of the deep convective cores shown in Fig. 1. The areas of low TSC, such as the Maritime Continent, South America and Central Africa align with the regions of high DCC occurrence. However the low TSC regions are more spread out around the regions of DCC occurrence, as they are advected via the wind field away from the initial DCC. Regions of particularly high TSC are the extra tropical regions around 30S and 30N latitudes, far from convection.

3.2 Evolution of ISCCP cloud properties

As the optically thick deep convective cores dissipate, a reduction in the cloud optical thickness (τ_c) is expected following previous studies (Luo and Rossow, 2004), as the anvil cirrus decays into thin cirrus and eventually disappears completely. Changes in the cloud top pressure (CTP) are also expected, moving from low pressure (high altitude) close to the convective core, to higher pressures (lower altitude) as the anvil cirrus extends and sinks (Luo and Rossow, 2004).

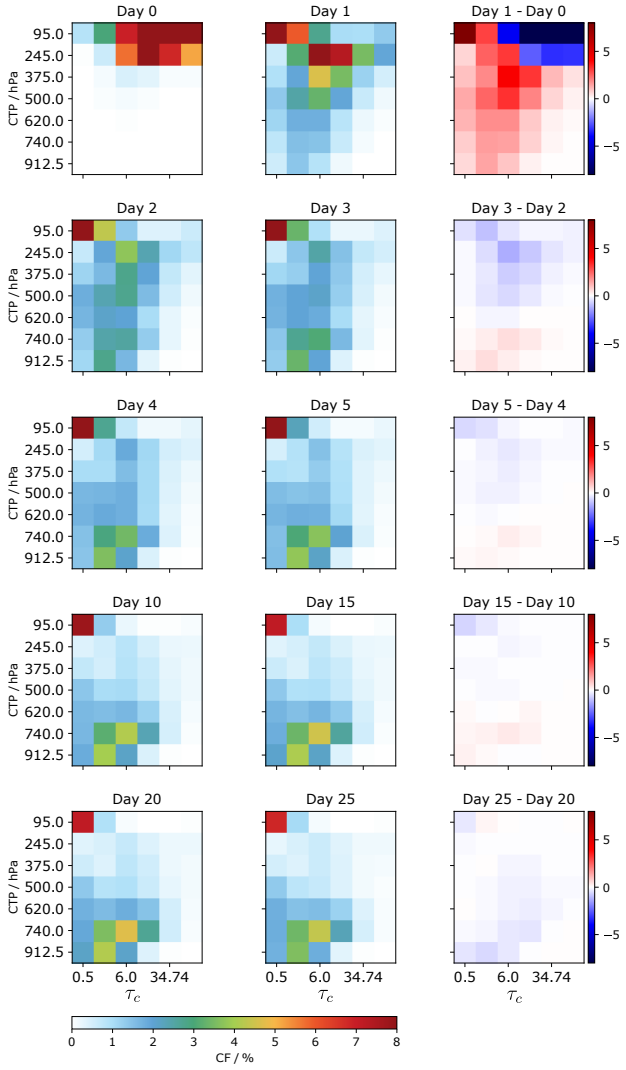

Figure 6. ISCCP-H joint histograms showing the distribution of the CTP, and τ_c and cloud fraction as a function of days since convection. The rightmost column shows the absolute percentage change between days. Day 0 is the first 0-24 hours since convection, day 1 is 24-48 hours since convection, and so on. High CF values for upper right gridboxes would indicate a distribution skewed towards optically thick, high altitude clouds, and the opposite (optically thin, low altitude), for bottom left.

Fig. 6 shows the ISCCP-H joint histograms in the first 5 days since convection, with each 24 hour period showing the joint histogram of CTP and τ_c. At Day 0 (0<TSC<24) the histogram is dominated by optically thick, high altitude clouds, with high cloud fractions. There is very little low cloud, which may be due to the thick high cloud obscuring the clouds below them. However, low clouds become visible in the first 24 hours since convection. There is a shift to optically thin clouds as TSC increases. This implies that the thick anvil cirrus clouds do not persist longer than 24 hours post convection, consistent with previous studies by Luo and Rossow (2004). This is supported by Fig. 6, showing the difference is largest between day 0 and day 1 than any subsequent day. High clouds with an optical thickness in the middle two bins (between 2.3 and 14.5) representing the thicker cirrus outflow are still noticeably persist up to day 5, with the most significant decrease in their cloud fraction happening 3 days after convection. They remain with low cloud fractions up to day 25.

From day 4 onwards, low clouds begin to dominate in the joint histogram, however there is still a presence of thin cirrus. Interestingly, small changes in the cloud fractions are still seen between day 10 and day 15, particularly an increase in low cloud and decrease in high cloud. This implies that the TSC is still influential at up to 360 hours from convection. Note that the top left bin (high, optically thin cloud) remains particularly frequent across all histograms. This is due to the failed retrievals. These can't be assigned into a particular τ_c/CTP bin and so are assigned into top left bin in the ISCCP-H dataset by default (Pincus et al., 2012), as mentioned in section 2.6.

These results are generally consistent with previous work (Gehlot and Quaas, 2012; Luo and Rossow, 2004), however this paper sees a slightly quicker decay of the anvil cirrus than in Luo and Rossow (2004), and continued changes in cloud fraction beyond 5 days from convection.

Luo and Rossow (2004) use a column averaged wind field between 200hPa-500hPa, whereas this work uses 200hPa-300hPa to better reflect the range of heights at which the anvil cirrus and detrained thin cirrus occur at. The wind field in this work will be on average faster than Luo and Rossow (2004), and therefore the air will travel further in the same period of time. As such a TSC value of 10 hours will be geographically further along the trajectory than in Luo and Rossow (2004). This will cause the lifetime of the convective outflow clouds to appear shorter in this work and may explain these differences to this work.

Seeing changes in the cloud fraction at such long TSC values is a consequence of the approach of this work. Unlike previous studies, where the trajectories were stopped at predetermined times, this work tracks air from convection for an unbounded amount of time. Therefore changes in cloud properties can be tracked at much longer times since convection than previous work, without having to pick out specific convective events that are known to reach a certain age. The TSC methodology also explicitly deals with scenarios in which a trajectory is overlapped by new convection.

3.3 Evolution of cloud properties

Fig. 7 shows the evolution of the CTP and τ_c respectively as a function of the TSC for both all cloud gridboxes (Fig. 7a,b) and the high cloud only gridboxes (Fig. 7c,d). The joint histograms are normalised so that the number of y-axis bins add up to unity, to account for the fact that there are more retrievals for smaller TSC values. This provides a higher temporal resolution than the histograms in Fig. 6.

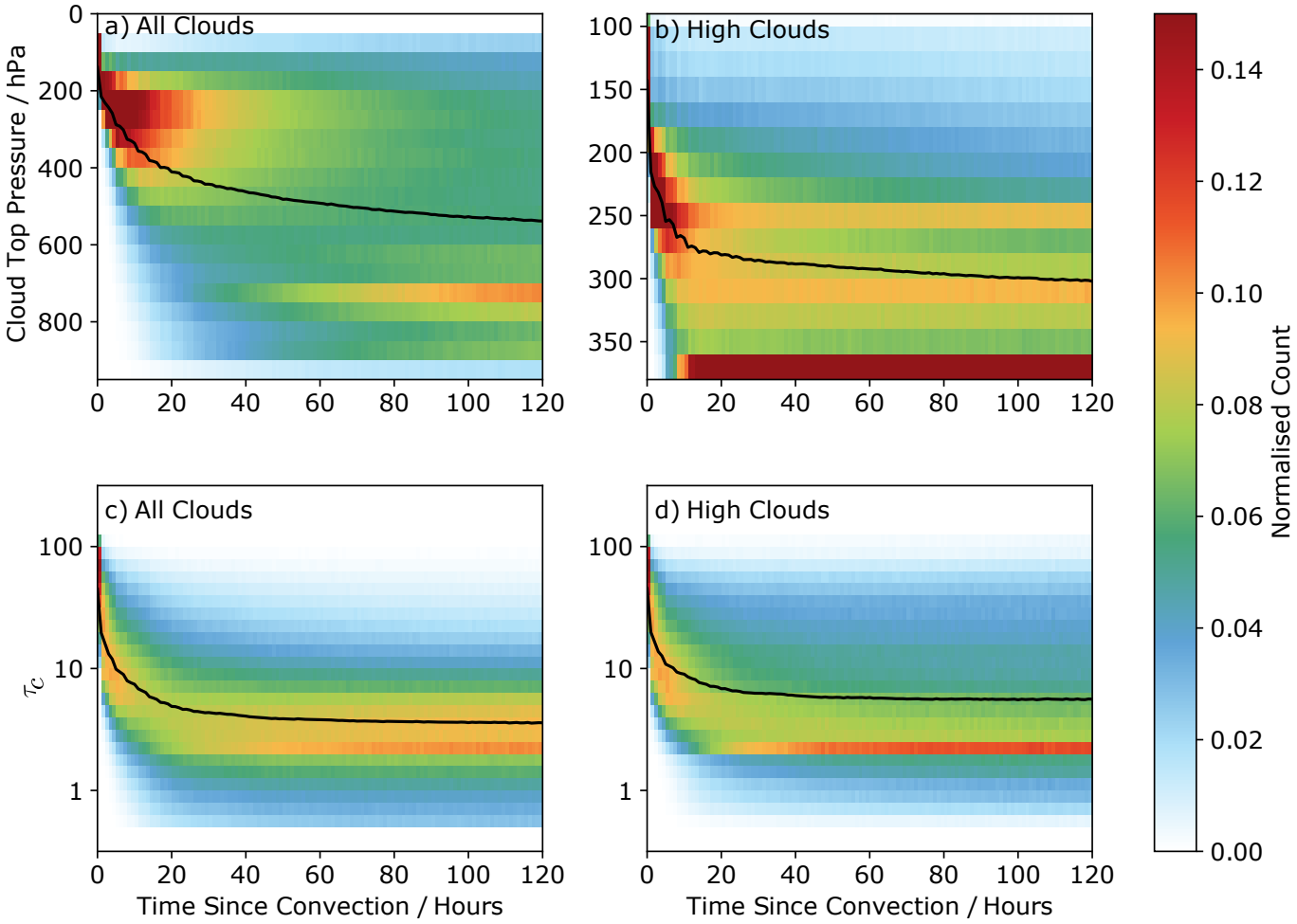

Figure 7. ISCCP cloud properties as a function of TSC. The normalised distribution represents the probability of finding clouds with a particular CTP or τ_c for a given TSC value. The black line indicates the mean value. Left-hand column shows the CTP and τ_c for all clouds, and right-hand column for high clouds only.

Fig. 7a shows that the CTP initially sits at very high altitudes for the convective cores, around 200hPa, coincident with the upper level wind field used. There is an large increase in the mean CTP in the first day since convection, as the convective core thins, and the mean CTP is skewed by the optically thicker lower altitude clouds (shown in Fig. 6). The histogram still shows a presence of higher altitude clouds, with an increasing proportion of low altitude clouds further from TSC-0 (the convection itself). There is still a decreasing CTP at 5 days from convection.

Isolating just the high clouds using the ISCCP histograms, Fig. 7b shows a similar decline in the mean CTP, albeit at lower pressures. The τ_c also sits at 200hPa initially, decaying to 250hPa in the first 6-12 hours as the convective core dissipates. The decay then slows, reaching 300hPa at 120 hours from convection. There is a significant cloud layer at 370hPa that becomes visible as the high cloud dissipates. These are likely clouds not associated with convection that become visible as the cloud fraction of the anvil cloud above decreases, and any changes in the properties of these clouds, particularly at large TSC values, are not suggested to be directly related to the initial convection.

Fig. 7c shows the evolution of the cloud optical thickness for all clouds. The all cloud τ_c drops significantly in the first 24 hours from convection, indicating the dissipation of the very thickest high clouds associated with the convective cores. This is to be expected as the regime shifts from thicker cirrus associated with convection, to thin cirrus that persists either after a convective event, or is formed in situ and unrelated to convection.

When just looking at high clouds in Fig. 7d, the mean values of the histogram are relatively unchanged. However there is larger spread in the cloud optical thicknesses, including a relative increase in the optically thinnest of the clouds in the lowest bin.

3.4 Vertical profile evolution

The vertical distribution of cloud and N_i vary strongly as a function of TSC. Fig. 8a shows the cloud amount and thus the general anvil shape of convective cores and their associated cirrus outflow up to 120 hours from convection. Fig. 8b shows the same up to 500 hours from convection. At very low TSC (TSC<2hr), there is a substantial amount of cloud at all altitudes up to approximately 16km associated with the very tops of the convective towers. The low to mid altitude cloud, likely the convective cores, quickly dissipates as the TSC increases. High clouds are maintained for much longer, with changes in the high cloud fraction continuing beyond 120 hours from convection. There is a moderate amount of low clouds, almost independent of TSC. There is also a sustained amount of mid level clouds between 4 and 8km for the first 60 hours. These mid level clouds are thought to form when latent heat associated with convective freezing creates a shallow temperature inversion which slows vertical motion in subsequent convective cycles and detrains moisture near the freezing level (Bourgeois et al., 2016). Fig. 8b shows that even at very long TSC values, beyond 120 hours up to 500 hours, there is still a significant change in cloud amount as a function of TSC.

Fig. 8c shows the ice crystal number concentration for particles greater than 5μm in diameter, (N_i^5), as a function of the time since convection. Fig. 8e shows the same as Fig. 8c but for those greater than 100μm, (N_i^{100}). Given that the N_i is a very strong function of temperature (and therefore altitude), it is useful to consider the relative changes in the N_i as a function of

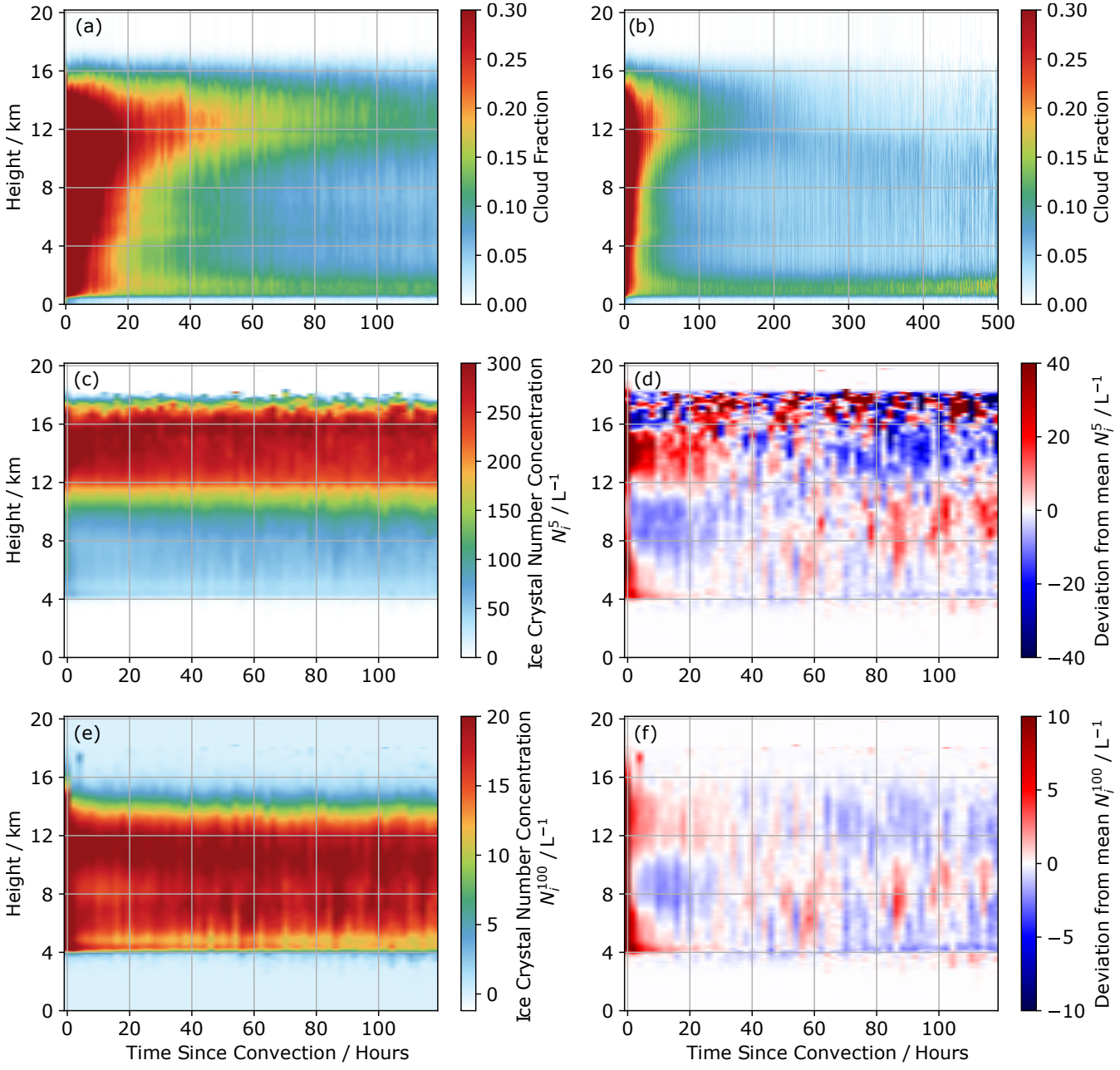

Figure 8. Vertical evolution of DARDAR cloud properties as a function of TSC. a) Cloud fraction up to 120 hours from convection. b) Cloud fraction up to 500 hours from convection. c) N_i for particles larger than 5μm. d) N_i^5 anomaly for 120 hours from convection. e) N_i for particles larger than 5μm. f) N_i^{100} anomaly from mean value for 120 hours from convection. Anomaly here refers to the difference in the N_i at a given TSC to the mean N_i at that altitude for the tropics.

TSC. Fig. 8d and 8e show the deviation of the N_i from the tropical mean N_i for a given altitude. Red indicates where the N_i at a given TSC is greater than the tropical mean, and blue those regions where it is less than the tropical mean.

Considering Fig. 8d first, there is an greater than average N_i^5 at all altitudes close to convection. This is most notable between 12km and 16km, where the N_i^5 peaks. This is to be expected given the presence of a deep convective core. At short times after TSC-0, there remains an above average N_i^5 between 12km and 16km. This is indicative of the convective outflow that remains after the convective core has dissipated. This outflow decays within 36-42 hours, when the deviation to the mean N_i^5 becomes negative. There is also an increase in N_i^5 at similar times at lower altitudes (between 4km and 8km) that decays within around 20 hours. This is likely due to the active shallow convection that occurs close to the region of deep convection, and thin mid level clouds discussed in Bourgeois et al. (2016). Considering Fig. 8f, there is a clear increase in the N_i^{100} close to convection, particularly at lower altitudes between 4km and 8km. Although the DARDAR retrieval is less reliable in convective cores (**?**), larger ice crystals are expected in the convective core at lower altitudes as they are less likely to be lifted higher into the cloud column than smaller ice crystals, and also subside quicker (Jensen et al., 2018). The lower altitude N_i^{100} drops off rapidly as the convective core dissipates. As in the case of the N_i^5, there is an increase in the N_i^{100} between 12km and 16km which is sustained for the first 24 hours from convection and linked to updrafts of large ice crystals from deep convective cores. In both of these figures there appears to be anomalies after 36-42 hours from clouds not directly detrained from convection. This is expected, as not all high clouds are detrained from convection or change as a function of TSC.

3.5 TSC as a function of latitude

It is clear from Fig. 5b) that on average TSC increases with latitude, expected from the large-scale behaviour of the Hadley circulation. However, while latitude can explain the broad features of the high cloud field, TSC offers valuable additional insight into the development of high clouds, more closely constraining their properties and development.

Fig. 9a) shows the zonally averaged DARDAR cloud fraction in the tropics for all gridboxes with a TSC value between 0 and 6 hours. Close to convection, it is clear there is very little latitudinal dependence in the cloud profile when when controlling for TSC. As TSC increases during the first 24 hours from convection (Figs. 9b,c), latitude starts to become relevant for determining the cloud profile, although the impact is still small. At three days from convection (Fig. 9d), the zonal cloud fraction begins to resemble the average tropical climatology **?**. Despite this, there as still clear changes in cloud fraction as a function of TSC at a given latitude, even several days after convection (Figs. 9e, f).

This demonstrates that the results shown in Fig. 8 are not purely due to the correlation between TSC and latitude. In contrast, TSC provides significant additional information about the state of the cloud field. In all regions of the tropics, the temporal evolution of clouds following convection is critical to understand high cloud properties.

3.6 Cloud radiative effects

The radiative evolution of convection, from thick convective core to thin anvil cirrus, is characterised by analysing the CERES SYN1deg L3 LW and SW TOA fluxes (NASA/LARC/SD/ASDC, 2017). Fig. 10 shows the SW, LW and net cloud radiative

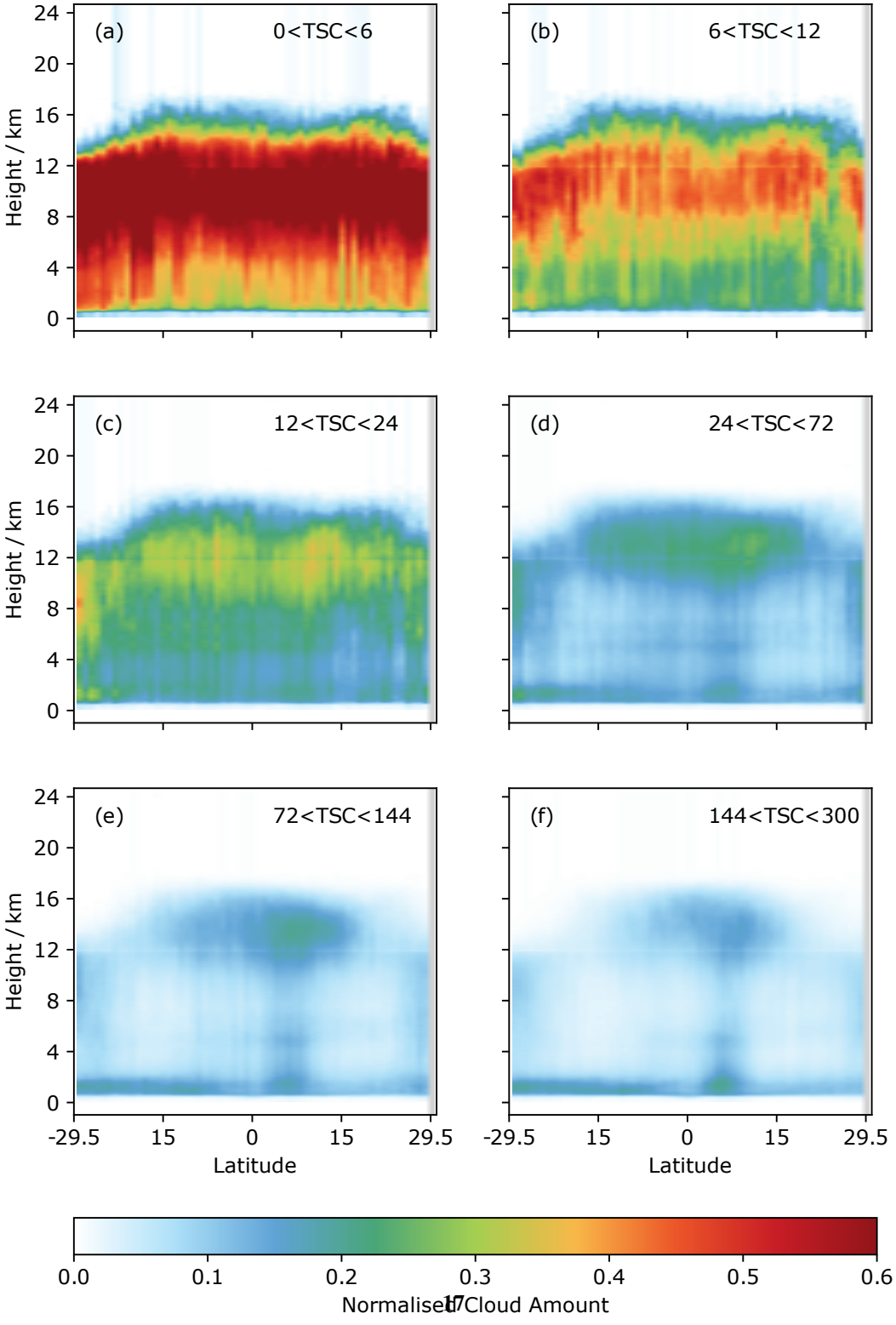
(a) 0<TSC<6
(b) 6<TSC<12
(c) 12<TSC<24
(d) 24<TSC<72
(e) 72<TSC<144
(f) 144<TSC<300
Height / km
0
4
8
12
16
20
24
-29.5
15
0
15
29.5
Latitude
0.0
0.1
0.2
0.3
0.4
0.5
0.6
Normalised Cloud Amount

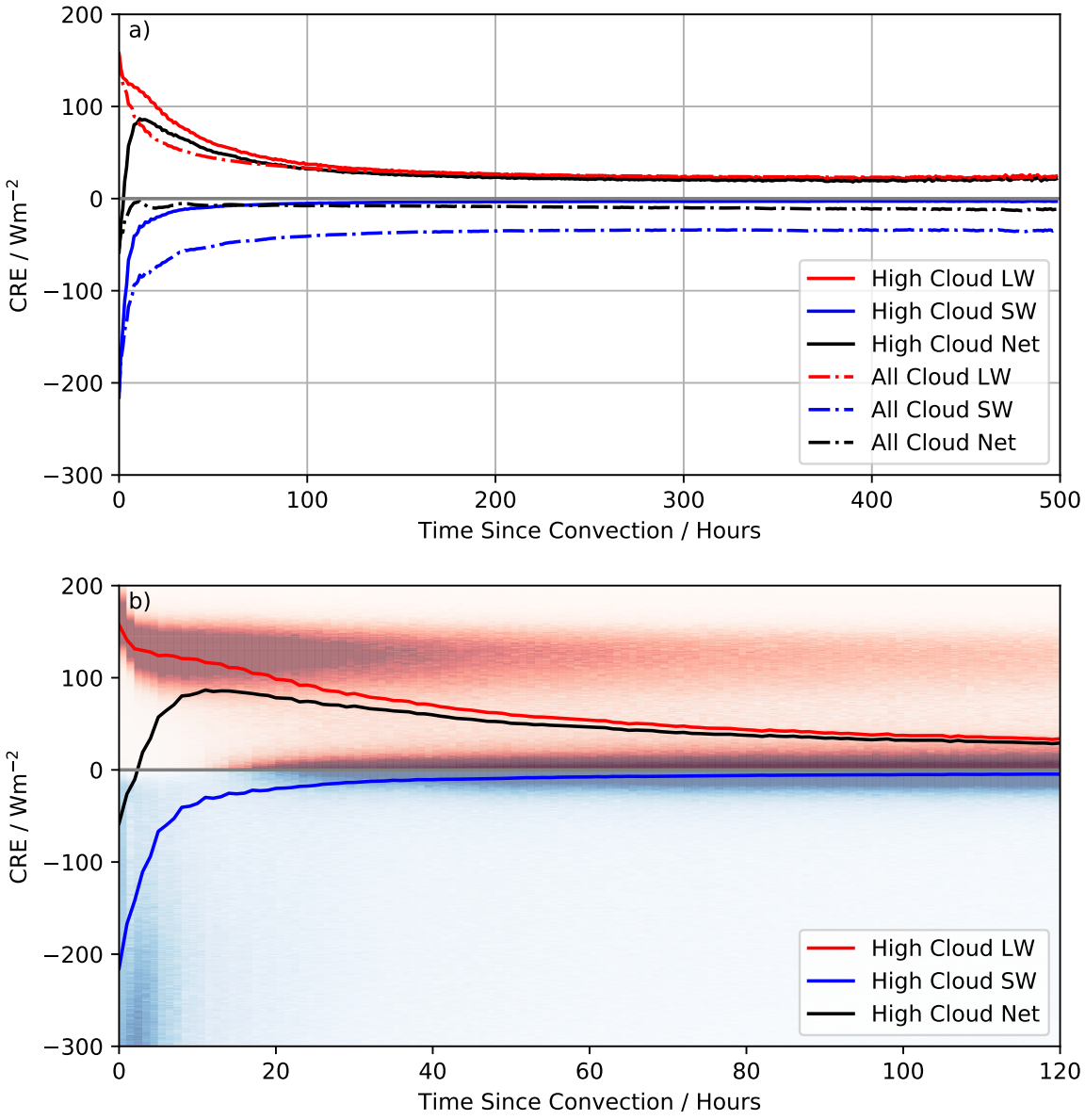

Figure 10. Cloud Radiative Effect (CRE) as a function of TSC. a) All cloud and high cloud LW, SW and Net CRE up to 500 hours from convection. b) High cloud LW, SW and Net CRE up to 120 hours from convection with normalised joint histogram the showing the probability of finding a particular CRE value (LW in red, SW in blue) for a given TSC value.

effect (CRE) as a function of the time since convection. Fig. 10a shows the evolution of the LW and SW and NET CRE for both the all cloud gridboxes, and gridboxes containing only high cloud, up to 500 hours from convection.

Fig. 10a shows that when considering the all cloud CRE, the net CRE is always slightly cooling, with an oscillation in the first 48 hours due to the diurnal cycle in the CRE. This net CRE of close to zero in the tropics is well studied (Ramanathan et al., 1989; Hartmann and Berry, 2017; Wielicki et al., 1996). In the all cloud case, there is initially a very large significant warming and cooling that cancel each other out. The LW and SW CRE decreases significantly in the first 24-48 hours as the cloud fraction of these clouds drop (Fig.8a). By 100 hours from convection there is very little change in the all cloud and high cloud CRE. To understand how the radiative forcing of the clouds that evolve from convection change, it is vital to consider only the gridboxes containing high clouds.

The high cloud CRE is a strong function of TSC at very low values of TSC (Fig. 10b). Initially, there is a large SW and LW component to the CRE, with -200Wm^{-2} SW cooling and 150Wm^{-2} LW warming at TSC-0, leading to a net CRE of -50Wm^{-2} cooling. This is due to the very optically thick convective core that reflects a significant portion of the incoming solar radiation (Fig.7d), whilst also having a very large LW warming due to its high cloud tops (Fig.7b).

As the convective core dissipates and the cloud optical thickness decreases, the SW CRE drops significantly, to 50Wm^{-2} at 6 hours from convection, whereas the LW warming remains 90Wm^{-2}. At this point, the net CRE shifts from a cooling regime to a warming regime, dominated by the LW warming of the thinner detrained cirrus. After the initial dissipation of the core, the net warming is sustained. By 24 hours since convection, the net CRE remains at 90Wm^{-2}, decreasing to 50Wm^{-2} at 120 hours from convection. The histogram in Fig. 10b shows the LW warming splitting into two layers, with the weighted mean value falling in between. The top layer, which sits at around 100Wm^{-1} is the high cirrus with a high cloud fraction that has the largest warming potential. The layer that emerges close to 0Wm^{-2} is due to the lower cloud fraction high clouds that emerge further from convection. These clouds may be directly detrained from convection themselves, but still evolve as a function of TSC. With their low cloud fraction, their CRE is small, close to 0Wm^{-2} in both the LW and SW.

This sustained warming as a function of TSC is not seen in previous studies. Gehlot and Quaas (2012) found the net CRE in the ECHAM5 model to be negative up to five days (120 hours) from convection. However they did not isolate the high clouds, meaning that cooling from lower altitude thick clouds contributed to their CRE. Without removing low clouds from the analysis, the work in this paper finds a similar sustained, albeit small, cooling for the all cloud CRE (Fig. 10).

Our results differ to previous model studies. Gasparini et al. (2021) looked at the CRE evolution in E3SM, a high resolution GCM. These results found that, after an initial positive CRE due to small insolation values where convection occurred early before sunrise. The SW and LW CRE quickly decayed, and the net CRE became negative after 2 hours, oscillating to a small warming again at 15 hours as the solar insolation decreased. These simulations did not represent the thinnest cirrus particularly well, so may underestimate some of the LW warming seen in this work.

4 Discussion

There are multiple benefits to the TSC approach described in this paper. It is computationally efficient when compared to tracking every single location of deep convection in the tropics. Instead of keeping and updating an array of locations for each new convective event, which grows with each timestep, this work has just one TSC array for the entire tropics, which is updated at each timestep. It also removes any bias in selecting specific initial convection, since all convection from the shortest lived to the longest lived contribute to the mean TSC. Finally, the unbounded nature of the tracking means that the full life cycle of all trajectories from convection are considered, until they are superseded by new convection.

However, there are some uncertainties introduced in the TSC algorithm. Firstly, it only considers horizontal wind fields, averaged between 200-300hPa, and there is no vertical advection of the TSC. This is a similar assumption as made by Luo and Rossow (2004), except that they considered a larger pressure averaged wind field between 200-500hPa. The choice of the 200-300hPa average wind field is supported by the evolution of the ISCCP CTP (Fig. 7), and the evolution of the HYSPLIT trajectory pressures. There is some vertical subsidence during the evolution of the cirrus, therefore using the 200-300hPa wind field means there is some uncertainty in the advection of the air from deep convection. Adding a vertical evolution component would be an option for future enhancement to the TSC algorithm. It would add considerable computational complexity, but would improve the calculations of TSC and reduce uncertainty introduced by using a pressure averaged wind field.

Secondly, there is necessary interpolation that occurs when the wind field diverges. If a grid box becomes empty between timesteps, then the value for the TSC in that grid box is calculated as the mean value of the surrounding grid boxes. This increases the uncertainty in longer TSC values. Two different interpolation methods have been tested, with minimal impact on the represented results, suggesting this is not a large source of uncertainty (see supplementary information).

While there are significant changes in DARDAR ice properties as a function of TSC (Fig.8), there are still considerable uncertainties surrounding the retrieval, particularly at warmer temperatures. The DARDAR-Nice Ni retrieval compares favourably to in-situ measurements at the cirrus temperatures that are the focus of this work (Sourdeval et al., 2018). However, the potential temporal variation of factors such as particle shape might introduce TSC-dependent biases in the Ni retrieval, producing an apparent change in Ni. This is will be investigated in future work.

Two key factors may introduce temporal biases in the CRE presented in Fig.10. First, to ensure CRE values existed for all clouds, missing LW clear sky values in the instantaneous data were filled with the 3 month/seasonal mean. This introduces some uncertainty into the results, but using annual averages makes little difference to the results. Using too short an averaging period results in large amounts of missing data near convection.

Secondly, the use of the ISCCP dataset to isolate the high cloud CRE was only possible during daylight hours, as the ISCCP joint histograms require cloud optical depth retrievals and so are only available during daylight. The SW CRE at night is known to be zero. However, as the high cloud LW CRE is not available at night, this work uses only the daytime LW CRE. This makes the implicit assumption that the high cloud LW CRE is similar for day and nighttime, this is a sensible assumption, particularly over the ocean which accounts for most of the area in the tropics. Future work could account for the missing data by using a radiative transfer model to explicitly calculate the nighttime CRE values (L'Ecuyer et al., 2008).

5 Conclusion

The lifecycle of convective cores and their associated cirrus outflows, including their vertical evolution, have been characterised in this paper through the creation of a "Time Since Convection (TSC)" dataset. Convection is identified in satellite data (Fig. 1), and then advected as a tracer in a reanalysis wind field, resulting in every point in the tropics being assigned a TSC value, indicating the last time that air parcel experienced convection (Fig. 4). Building on previous studies that were forced to set an artifical limit to the time they tracked a parcel of air from convection (Luo and Rossow, 2004; Gehlot and Quaas, 2012), the methodology presented here allows an effectively unbounded upper limit for the time since convection. Changes in high clouds as a function of TSC continue to be observed several days after the convective event (Figs 9).

Cloud properties are strong functions of TSC, particularly those for high clouds. There is a general trend for high altitude, optically thinner clouds to appear over time, as expected in the evolution of deep convection to anvil to thin cirrus (Fig. 7). Following a sharp initial decay in both the CTP and COT in the first 12 hours from convection, a slower decrease is observed in ISCCP data over the next 120 hours. This gradual thinning of the anvil is also seen in vertical profiles of cloudiness, with the clearest changes observed in the first 120 hours (Fig. 8a), although changes in cloud fraction as a function of TSC continue to be observed for several hundred hours after the convective event (Fig. 8b).

Cloud properties and TSC are both strong functions of latitude in the tropics (Fig. 4. However, changes in the cloud properties along TSC trajectories are not solely due to latitudinal changes along these trajectories. Controlling for latitude by looking at the zonally averaged cloud amount at a given TSC, it is clear that cloud properties are similar for a given TSC at all latitudes. This shows that looking at evolution along trajectories is not merely characterising the changing climatology as trajectories move from tropics to extra tropics, but it provides significant extra information on cloud evolution, making it a powerful tool for studying the development of clouds.

The changes in cloud properties explain the observed evolution of the CRE as a function of TSC (Fig. 10). Considering the CRE for all clouds, the net CRE is very close to zero at all values of TSC. This apparent balance in the tropical CRE is well documented (Wielicki et al., 1996; Ramanathan et al., 1989; Hartmann and Berry, 2017), occuring both close to convection when the the LW and SW values are very high and at very large TSC. However, when the high cloud only regions are isolated, there is a sustained warming beyond 120 hours from convection after a brief initial cooling. The warming effect of high clouds is only unmasked when removing the optically thick, low clouds from the analysis, which generate a significant SW cooling at large TSC (Fig. 7). The LW warming from these high, optically thin clouds is sustained well beyond 24 hours from convection, by which point the SW cooling from the convective core has largely dissipated. With this close CRE balance at a range of TSC values, understanding the controls on high cloud evolution as a function of TSC is essential to constrain the processes governing tropical radiation balance.

This paper has introduced a novel method for assessing the evolution of clouds following convection, through anvil cirrus to thin cirrus. Combining satellite and reanalaysis data to calculate the "time since convection" for each point in the tropics, this provides a new window into high cloud development in the tropics. The flexible nature of the TSC approach allows it to be easily applied to a wide range of cloud and atmospheric datasets. Whilst there are significant changes in CRE with TSC

observed close to convection, this work also also demonstrates that changes in cloud properties with TSC can be observed at timescales up to 500 hours from convection, long after the original convective event has dissipated. With previous studies being limited to the youngest 30% of tropical locations (<120 hours), there is a clear need for future investigation of cirrus development at these longer timescales.

Author contributions. Both authors contributed to study design and interpretation of results. GH performed the analysis and prepared the manuscript, with comments from EG.

Competing interests. The contact author has declared that neither they nor their co-author has any competing interests.

Acknowledgements. This work was supported by a Royal Society University Research Fellowship (URF\R1\191602) and a PhD studentship from the Department of Physics, Imperial College London. The authors gratefully acknowledge the NOAA Air Resources Laboratory (ARL) for the provision of the HYSPLIT transport and dispersion model and READY website (https://www.ready.noaa.gov) used in this publication. The authors also gratefully acknowledge Odran Sourdeval and Athulya Saiprakash (University of Lille) for providing the DARDAR data, and for helpful discussions and suggestions.

References

Berry, E. and Mace, G. G.: Cloud properties and radiative effects of the Asian summer monsoon derived from A-Train data, Journal of Geophysical Research: Atmospheres, 119, 9492–9508, https://doi.org/10.1002/2014JD021458, 2014.

Bourgeois, Q., Ekman, A. M. L., Igel, M. R., and Krejci, R.: Ubiquity and impact of thin mid-level clouds in the tropics, Nature Communications, 7, 12 432, https://doi.org/10.1038/ncomms12432, 2016.

Choi, Y.-S. and Ho, C.-H.: Radiative effect of cirrus with different optical properties over the tropics in MODIS and CERES observations, Geophysical Research Letters, 33, https://doi.org/10.1029/2006GL027403, 2006.

Delanoë, J. and Hogan, R. J.: A variational scheme for retrieving ice cloud properties from combined radar, lidar, and infrared radiometer, Journal of Geophysical Research: Atmospheres, 113, https://doi.org/10.1029/2007JD009000, 2008.

Fan, J., Leung, L. R., Rosenfeld, D., Chen, Q., Li, Z., Zhang, J., and Yan, H.: Microphysical effects determine macrophysical response for aerosol impacts on deep convective clouds, Proceedings of the National Academy of Sciences, 110, E4581–E4590, https://doi.org/10.1073/pnas.1316830110, 2013.

Garrett, T. J., Navarro, B. C., Twohy, C. H., Jensen, E. J., Baumgardner, D. G., Bui, P. T., Gerber, H., Herman, R. L., Heymsfield, A. J., Lawson, P., Minnis, P., Nguyen, L., Poellot, M., Pope, S. K., Valero, F. P. J., and Weinstock, E. M.: Evolution of a Florida Cirrus Anvil, Journal of the Atmospheric Sciences, 62, 2352 – 2372, https://doi.org/10.1175/JAS3495.1, 2005.

Gasparini, B., Blossey, P. N., Hartmann, D. L., Lin, G., and Fan, J.: What Drives the Life Cycle of Tropical Anvil Clouds?, Journal of Advances in Modeling Earth Systems, 11, 2586–2605, https://doi.org/10.1029/2019MS001736, 2019.

Gasparini, B., Rasch, P. J., Hartmann, D. L., Wall, C. J., and Dütsch, M.: A Lagrangian Perspective on Tropical Anvil Cloud Lifecycle in Present and Future Climate, Journal of Geophysical Research: Atmospheres, 126, e2020JD033 487, https://doi.org/10.1029/2020JD033487, e2020JD033487 2020JD033487, 2021.

Gehlot, S. and Quaas, J.: Convection-Climate Feedbacks in the ECHAM5 General Circulation Model: Evaluation of Cirrus Cloud Life Cycles with ISCCP Satellite Data from a Lagrangian Trajectory Perspective, Journal of Climate, 25, 5241 – 5259, https://doi.org/10.1175/JCLI-D-11-00345.1, 2012.

Harrison, E. F., Minnis, P., Barkstrom, B. R., Ramanathan, V., Cess, R. D., and Gibson, G. G.: Seasonal variation of cloud radiative forcing derived from the Earth Radiation Budget Experiment, Journal of Geophysical Research: Atmospheres, 95, 18 687–18 703, https://doi.org/10.1029/JD095iD11p18687, 1990.

Hartmann, D. L. and Berry, S. E.: The balanced radiative effect of tropical anvil clouds, Journal of Geophysical Research: Atmospheres, 122, 5003–5020, https://doi.org/10.1002/2017JD026460, 2017.

Hartmann, D. L., Holton, J. R., and Fu, Q.: The heat balance of the tropical tropopause, cirrus, and stratospheric dehydration, Geophysical Research Letters, 28, 1969–1972, https://doi.org/10.1029/2000GL012833, 2001a.

Hartmann, D. L., Moy, L. A., and Fu, Q.: Tropical Convection and the Energy Balance at the Top of the Atmosphere, Journal of Climate, 14, 4495 – 4511, https://doi.org/10.1175/1520-0442(2001)014<4495:TCATEB>2.0.CO;2, 2001b.

Hersbach, H., Bell, B., Berrisford, P., Biavati, G., Horányi, A., Muñoz Sabater, J., Nicolas, J., Peubey, C., Radu, R., Rozum, I., Schepers, D., Simmons, A., Soci, C., Dee, D., and Thépaut, J.-N.: ERA5 hourly data on pressure levels from 1959 to present., https://doi.org/10.24381/cds.bd0915c6, 2018.

Jensen, E. J., van den Heever, S. C., and Grant, L. D.: The Life Cycles of Ice Crystals Detrained From the Tops of Deep Convection, Journal of Geophysical Research: Atmospheres, 123, 9624–9634, https://doi.org/10.1029/2018JD028832, 2018.

Kiehl, J. T.: On the Observed Near Cancellation between Longwave and Shortwave Cloud Forcing in Tropical Regions, Journal of Climate, 7, 559–565, https://doi.org/10.1175/1520-0442(1994)007<0559:OTONCB>2.0.CO;2, 1994.

Klein, S. A. and Jakob, C.: Validation and Sensitivities of Frontal Clouds Simulated by the ECMWF Model, Monthly Weather Review, 127, 2514 – 2531, https://doi.org/https://doi.org/10.1175/1520-0493(1999)127<2514:VASOFC>2.0.CO;2, 1999.

Koren, I., Remer, L. A., Altaratz, O., Martins, J. V., and Davidi, A.: Aerosol-induced changes of convective cloud anvils produce strong climate warming, Atmospheric Chemistry and Physics, 10, 5001–5010, https://doi.org/10.5194/acp-10-5001-2010, 2010.

Krämer, M., Rolf, C., Luebke, A., Afchine, A., Spelten, N., Costa, A., Meyer, J., Zöger, M., Smith, J., Herman, R. L., Buchholz, B., Ebert, V., Baumgardner, D., Borrmann, S., Klingebiel, M., and Avallone, L.: A microphysics guide to cirrus clouds – Part 1: Cirrus types, Atmospheric Chemistry and Physics, 16, 3463–3483, https://doi.org/10.5194/acp-16-3463-2016, 2016.

Luo, Z. and Rossow, W. B.: Characterizing Tropical Cirrus Life Cycle, Evolution, and Interaction with Upper-Tropospheric Water Vapor Using Lagrangian Trajectory Analysis of Satellite Observations, Journal of Climate, 17, 4541 – 4563, https://doi.org/10.1175/3222.1, 2004.

L'Ecuyer, T. S., Wood, N. B., Haladay, T., Stephens, G. L., and Stackhouse, P. W.: Impact of clouds on atmospheric heating based on the R04 CloudSat fluxes and heating rates data set, Journal of Geophysical Research: Atmospheres, 113, https://onlinelibrary.wiley.com/doi/abs/10.1029/2008JD009951, 2008.

Mace, G. G., Deng, M., Soden, B., and Zipser, E.: Association of Tropical Cirrus in the 10–15-km Layer with Deep Convective Sources: An Observational Study Combining Millimeter Radar Data and Satellite-Derived Trajectories, Journal of the Atmospheric Sciences, 63, 480–503, https://doi.org/10.1175/JAS3627.1, 2006.

Massie, S., Gettelman, A., Randel, W., and Baumgardner, D.: Distribution of tropical cirrus in relation to convection, Journal of Geophysical Research: Atmospheres, 107, AAC 19–1–AAC 19–16, https://doi.org/10.1029/2001JD001293, 2002.

NASA/LARC/SD/ASDC: CERES and GEO-Enhanced TOA, Within-Atmosphere and Surface Fluxes, Clouds and Aerosols 1-Hourly Terra-Aqua Edition4A, 10.5067/TERRA+AQUA/CERES/SYN1DEG-1HOUR_L3.004A, 2017.

Pincus, R., Platnick, S., Ackerman, S. A., Hemler, R. S., and Hofmann, R. J. P.: Reconciling Simulated and Observed Views of Clouds: MODIS, ISCCP, and the Limits of Instrument Simulators, Journal of Climate, 25, 4699 – 4720, https://doi.org/10.1175/JCLI-D-11-00267.1, 2012.

Protopapadaki, S. E., Stubenrauch, C. J., and Feofilov, A. G.: Upper tropospheric cloud systems derived from IR sounders: properties of cirrus anvils in the tropics, Atmospheric Chemistry and Physics, 17, 3845–3859, https://doi.org/10.5194/acp-17-3845-2017, 2017.

Ramanathan, V., Cess, R. D., Harrison, E. F., Minnis, P., Barkstrom, B. R., Ahmad, E., and Hartmann, D.: Cloud-Radiative Forcing and Climate: Results from the Earth Radiation Budget Experiment, Science, 243, 57–63, https://doi.org/10.1126/science.243.4887.57, 1989.

Riihimaki, L. D., McFarlane, S. A., Liang, C., Massie, S. T., Beagley, N., and Toth, T. D.: Comparison of methods to determine Tropical Tropopause Layer cirrus formation mechanisms, Journal of Geophysical Research: Atmospheres, 117, https://doi.org/10.1029/2011JD016832, 2012.

Rolph, G., Stein, A., and Stunder, B.: Real-time Environmental Applications and Display sYstem: READY, Environmental Modelling and Software, 95, 210–228, https://doi.org/10.1016/j.envsoft.2017.06.025, 2017.

Rossow, W., Golea, V., Walker, A., Knapp, K., Young, A., Hankins, B., and Inamdar, A.: International Satellite Cloud Climatology Project (ISCCP) Climate Data Record, H-Series, https://doi.org/10.7289/V5QZ281S, 2017.

Salathé, E. P. and Hartmann, D. L.: A Trajectory Analysis of Tropical Upper-Tropospheric Moisture and Convection, Journal of Climate, 10, 2533–2547, http://www.jstor.org/stable/26243410, 1997.

Schwartz, M. C. and Mace, G. G.: Co-occurrence statistics of tropical tropopause layer cirrus with lower cloud layers as derived from CloudSat and CALIPSO data, Journal of Geophysical Research: Atmospheres, 115, https://doi.org/10.1029/2009JD012778, 2010.

Sourdeval, O., Gryspeerdt, E., Krämer, M., Goren, T., Delanoë, J., Afchine, A., Hemmer, F., and Quaas, J.: Ice crystal number concentration estimates from lidar–radar satellite remote sensing – Part 1: Method and evaluation, Atmospheric Chemistry and Physics, 18, 14 327–14 350, https://doi.org/10.5194/acp-18-14327-2018, 2018.

Tselioudis, G., Rossow, W. B., Jakob, C., Remillard, J., Tropf, D., and Zhang, Y.: Evaluation of Clouds, Radiation, and Precipitation in CMIP6 Models Using Global Weather States Derived from ISCCP-H Cloud Property Data, Journal of Climate, 34, 7311 – 7324, https://doi.org/10.1175/JCLI-D-21-0076.1, 2021.

Wall, C. J. and Hartmann, D. L.: Balanced Cloud Radiative Effects Across a Range of Dynamical Conditions Over the Tropical West Pacific, Geophysical Research Letters, 45, 11,490–11,498, https://doi.org/10.1029/2018GL080046, 2018.

Wall, C. J., Hartmann, D. L., Thieman, M. M., Smith, W. L., and Minnis, P.: The lifecycle of anvil clouds and the top-of-atmosphere radiation balance over the tropical west Pacific, Journal of climate, 31, 10 059–10 080, https://doi.org/10.1175/jcli-d-18-0154.1, 2018.

Wielicki, B. A., Barkstrom, B. R., Harrison, E. F., Lee, R. B., Smith, G. L., and Cooper, J. E.: Clouds and the Earth's Radiant Energy System (CERES): An Earth Observing System Experiment, Bulletin of the American Meteorological Society, 77, 853–868, https://doi.org/10.1175/1520-0477(1996)077<0853:CATERE>2.0.CO;2, 1996.